scientific reports

Check for updates

OPEN

Laser based 100 GeV electron acceleration scheme for muon production

J. D. Ludwig[1,6]✉, S. C. Wilks[1], A. J. Kemp[1], G. J. Williams[1], N. Lemos[1], E. Rockafellow[2], B. Miao[2], J. E. Shrock[2], H. M. Milchberg[2], J.-L. Vay[3], A. Huebl[3], R. Lehe[3], A. Cimmino[4], R. Versaci[4], S. V. Bulanov[4], P. Valenta[4], V. Tang[1] & B. A. Reagan[1,5]

High energy muons, due to their unique ability to penetrate deeply into matter, can enable radiography of structures that cannot be probed by other forms of radiation. Current terrestrial sources of muons require conventional GeV-TeV particle accelerators which are hundreds to thousands of meters in size. Laser wakefield acceleration (LWFA) can achieve acceleration gradients of two-to-three orders of magnitude greater than conventional accelerators, thus shrinking the accelerator to a number of meters. We propose a concept for a compact muon source based on the first self-consistent PIC simulations of an all optical LWFA that uses a guiding channel to achieve electron energies of 100 GeV in a distance of 6 m with a driving laser energy of 300 J in a single stage. From the resulting electron energy spectrum we estimate muon production for this source. We show that this accelerator, coupled with high average power laser driver technology, provides the basis for a high energy and high flux muon source.

In the late 1960s Luis Alvarez[1] proposed using high energy muons to image through dense objects. Since muons have approximately 200 times the mass of electron and both particles primarily lose energy via bremsstrahlung, for the same initial energy it takes a longer distance for muons to be stopped in a material. As a practical example of this, muons have been used to scan the great pyramid of Giza revealing a previously unknown interior chamber[2]. This application relied on cosmic ray generated muons to detect a void within 100 m of limestone. Cosmic ray muons have also been used to examine the interior of the Fukushima Daiichi nuclear reactor[3] and for cargo container inspection[4]. However, the low flux of cosmic ray muons of about 1/cm^2/min at sea level and their inherent vertical directionality have limited their use in many practical applications. Conventional GeV-TeV particle accelerators are good sources of artificial muons[5] but their kilometer-scale size limits application utility.

Laser wakefield acceleration (LWFA) is a specific type of laser-based plasma accelerator (LPA) first proposed in 1979[6]. LWFA can achieve acceleration gradients up to 100 GeV/m, which is 1000 times greater than typical RF accelerators. Recent experiments have demonstrated electron energies of 5–10 GeV[7–9]. While the idea for using LWFA to generate a muon source has previously been proposed[10–12], that work considered electron energies only up to 10 GeV and did not contain modeling of the LWFA. Modeling of LWFA electron acceleration up to 40 GeV has previously been published[13]; however their simulations did not include electron self-injection. In this article, we present results of the first detailed physics-based simulations and modeling of an all optical LPA that reaches 100 GeV. Coupled with new laser architectures under development[14] that are efficient, high average power, and relatively compact, this muon source has the potential to be transportable, thus opening up a wide range of applications. Key elements of the source that make this possible are an optical waveguide[9,15–19] for the driver laser pulse, ionization injection to load the wake, and including a ramp[20,21] in the plasma density to combat dephasing of the electrons in the accelerating wake.

The basis for a LWFA is that a short laser pulse is injected into a low density plasma. The ponderomotive force of the pulse expels electrons from the optical axis, driving a wave (wake) in the plasma as electrons oscillate about the optical axis after transmission of the pulse. The alternating regions of positive and negative charge density produce strong electric fields (wakefields) with components directed longitudinally along the optical axis (accelerating/decelerating fields) and transversely (focusing fields)". For the most part, prior research[22–24]

[1]Lawrence Livermore National Laboratory, 7000 East Avenue, Livermore, CA 94551, USA. [2]Institute for Research in Electronics and Applied Physics and Department of Physics, University of Maryland, College Park, MD 20742, USA. [3]Lawrence Berkeley National Laboratory, 1 Cyclotron Road, Berkeley, CA 94720, USA. [4]ELI Beamlines Facility, The Extreme Light Infrastructure ERIC, Za Radnicí 835, 252 41 Dolní Břežany, Czech Republic. [5]Present address: Department of Electrical and Computer Engineering, Colorado State University, Fort Collins, Colorado 80521, USA. [6]Present address: Xcimer Energy, 10325 E 47th Ave, Denver, Colorado 80238, USA. ✉email: josh_ludwig@live.com

into this class of accelerator has focused on creating electron beams suitable for high energy physics applications where great effort has gone into attempting to create beams where all electrons are high energy (>>1 GeV), mono-energetic ($< 1\%\Delta$E/E relative energy spread), very low emittance (<10 um-mrad), and moderate charge (pC). Applications of LWFA for X-ray light sources have slightly relaxed constraints but a low beam emittance is still preferred[25].

By contrast, muon generation requires only high energy electrons (> 1 GeV) and as high beam charge as possible. Since muon generation is not concerned with a low emittance, or mono-energetic beam, the possibility of moving to the highly nonlinear "bubble" regime[26,27] as shown in Fig. 1 is desirable. In the nonlinear bubble regime, it is common to get a broad energy spectrum of electrons, depending on the method that the electrons are loaded into the wave. The nonlinear acceleration inside of waveguides is a unique and relatively understudied regime that offers distinct advantages over the linear regime. For example, an advantage of working in the bubble regime, as opposed to the linear regime, is that the accelerating fields are typically much larger. This translates to shorter accelerator lengths to achieve a given peak energy, which is ideal for reducing the footprint and thus increasing the mobility of the accelerator. The predictive scaling laws given in Lu et al.[26,27] are useful guides to determine accelerator output values as a function of given laser parameters with the assumption of a uniform plasma density along the accelerating length and minimal drive laser dispersion. However, once these assumptions are no longer valid (nonlinear evolution of the laser pulse, red shifting of the laser pulse, nonlinear evolution of the density profile, and non-optimal beam diameters) it is important to perform detailed modeling, as the dynamics of the injection and subsequent electron motion are highly nonlinear.

In addition to the LWFA blowout regime being the ideal method of electron acceleration for a compact muon source due to the shorter acceleration distances, it is also beneficial in that there is the possibility of much higher amount of charge per bunch when the constraint of requiring a monoenergetic beam is removed. In the blowout regime there are several methods of injecting electrons into the accelerating wave where they are sourced directly from the background plasma. Two common methods of electron injection are "down-ramp injection"[28,29] and "ionization injection"[30,31], we will focus on the latter. In particular, we will show that with global, or continuous ionsization injection (where the dopant gas is present throughout the entire length of the plasma), a significant amount of charge can be accelerated between a few MeV and up to some peak energy in the several to 100 GeV range. When directed into a high Z converter target, these electrons produce an intense shower of gammas with similar energies that then produce pions[32,33]. The main mechanism of muon generation is via the decay of these photoproduced pions. Another mechanism for muon creation is Bethe–Heitler muon pair production[34]. The resulting muons have a large Lorentz boost in the incident electron direction and this results in a relatively narrow beam divergence. Therefore, LWFA in the blowout regime with global electron injection is an ideal method to produce a strong muon source.

While the blowout regime is attractive for muon generation, it has been found that working in the transition region (where $a_0 \sim 1 - 3$) between the highly nonlinear and linear regime has some distinct advantages such as more efficient use of the laser energy[35,36]. Recent experiments in this intermediate regime by the University of Maryland (UMD) and Colorado State University (CSU) using the ALEPH laser[37] have been successful in achieving multi-GeV electron beams in a short distance using ionization injection and a modest laser energy[9,18,38,39]. In these experiments the acceleration length is increased by using an optically formed plasma waveguide. This waveguide, which requires a second low power laser pulse (1-2 Joules in 100-200 fs) focused by a diffractive axicon lens to create a Bessel beam, was crucial in obtaining up to 5-7 GeV electron beams over a distance of just 20 cm using a ~15 J laser.

The efficiency of muon conversion is $\sim 10^{-6} - 10^{-4}$ for 1–100 GeV electron beams in cm-thick high Z converter targets[40]. In order to generate sufficient muon flux for applications therefore requires a high flux of high energy electrons. Current multi-GeV LWFA experiments have produced 100 pC to nC of total charge. As

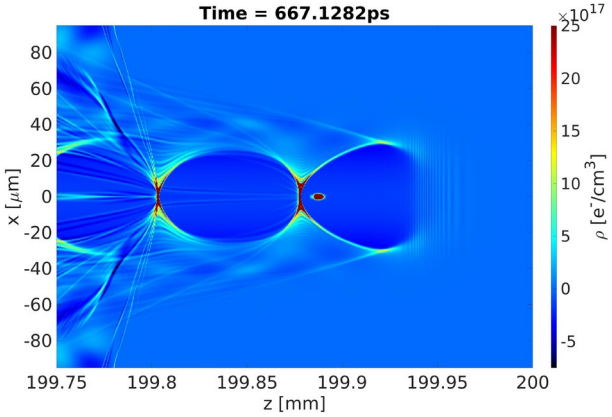

Fig. 1. Cross-section of a 3D simulation showing the plasma charge density ρ in units of electron charge per cubic centimeter at time = 667 ps into the simulation. The accelerated electron bunch resulting from localized injection is viable in the back of the first bubble. The laser (not shown) travels from left to right and is primarily contained within the right half of the right-most bubble. This figure is an illustration of a 3D Cartesian simulation of Run 1 in Table 1. The simulation domain was 256 μm *times* 256 μm x 4096 μm.

discussed below, increasing the bunch charge per shot combined with high repetition rate laser drivers currently under development[14] will allow the production of high energy muons at a flux many orders of magnitude above the natural cosmic ray-generated muon flux.

Results and discussion

Approach for obtaining 100 GeV electrons

As described above, the natural starting point is to work close to the nonlinear blowout regime. While this does indeed predict a more efficient way to achieve an increase in the maximum electron energy obtainable over what is expected for the linear regime (for a given laser energy) there is an additional gain to be realized by longitudinally ramping the density[41,42] of the plasma waveguide[43]. By ramping up the plasma density in the direction of laser propagation, the size of the accelerating "bucket" shrinks thereby allowing it to keep up with the accelerating electron bunch as it moves into the higher density. This allows the acceleration length to exceed its dephasing limit. The increased plasma density also results in a stronger electric field and so results in higher final electron energies for a given length of plasma.

The energy gain for the blowout regime can be expressed as[26,27]

$$\Delta E = (n_{cr}/n_e)^{2/3}(P/m_e^2c^5/e^2)^{1/3}m_ec^2 \tag{1}$$

where ΔE is the electron energy gain, n_{cr} is the critical electron density, n_e is the plasma electron density, P is the laser power, m_e is the electron mass, e is the fundamental charge, and c is the speed of light in a vacuum. It is valid for both self-guided[44] laser pulses and those in waveguides, the maximum length will be determined by either dephasing or pump depletion. From this equation it is clear that there are two ways to increase the maximum energy. Either increase the laser power or decrease the plasma density. If we assume that for a given set of laser and plasma parameters for a particular facility the laser power is already nearly optimized we can start our scaling study by decreasing the plasma density which is a simple route to higher energy electrons. For example, consider decreasing the density by a factor of 2. This means that in order to scale from the original parameters, we increase the spot size of the laser pulse w_0 to keep it matched to a fraction of the plasma wavelength given by

$$k_p w_0 \leq 2\sqrt{a_0}. \tag{2}$$

where $k_p = 2\pi c/\omega_{pe}$ is the plasma wave-number, and $a_0 = eE/m_ec\omega_0$ is the normalized laser field amplitude. In order to match the laser length to the new (longer) plasma wavelength, the pulse length must also be increased by the square root of 2. These 2 factors result in an increase of laser energy.

Waveguides are employed to mitigate pulse diffraction and enable acceleration up to the dephasing length which is given by

$$L_{dp} \approx 4/3\frac{\omega_0^2}{\omega_{pe}^2}\sqrt{a_0}k_p^{-1} \tag{3}$$

where L_{dp} is the maximum length of plasma over which acceleration can occur. It is found that when the Lu scaling is done for a constant density plasma, the distance required to achieve 100 GeV is 18 m, a length too long to be compatible with a transportable source (for reference a semi-truck trailer is 16 m). One solution to this problem is to ramp the plasma density up in the direction of laser pulse propagation as discussed above. To start, we consider a linear density ramp of

$$n_e(z) = n_0(1 + C_0 z/L_z) \tag{4}$$

where $C_0 = 2$ and L_z is the length of the plasma along the laser propagation direction. This density ramp allows for a given electron energy gain to take place in a shorter length. In effect, the increasing density results in an increasing accelerating gradient and therefore the total energy gain can be obtained in a shorter distance, in addition to allowing more of the electron bunch to stay in phase with the accelerating portion of the wake.

As scaling towards 100 GeV electron energies continues, it is found that the use of preformed channels significantly lowers the required laser power. This lower energy requirement results from being able to operate at a lower a_0 for a given set of plasma conditions. Physically, this lower power requirement (for a fixed plasma density, which is equivalent to a fixed pulse length when one considers the optimal pulse length) arises because for a pre-formed channel, the driving laser pulse expends less energy to expel electrons from the bubble region, as the central channel region contains less plasma. A preformed channel also helps to inhibit the beam from breaking into filaments by lowering the energy requirement, since the operating a_0 for a given set of plasma condition can be lowered. In this manuscript we present results that take advantage of a preformed channel due the benefits described above. It is also theoretically possible to self guide a laser, however, in our initial simulations of self guided pulses we observed catastrophic laser filamentation far before the required acceleration distance.

The choice of ionization injection[30] as the mechanism to load the accelerating wave up with electrons allows the use of a single laser for both injection and acceleration. This method was successfully demonstrated in recent experiments[16] and related simulations[43] and we adopt this as the starting point for this study. We report on cases where the dopant gas is present throughout the length of the plasma, and a case with a localized injection technique where the dopant gas is localized to a thin layer of nitrogen doped gas which is present near the beginning of the accelerator[30], which results in a quasi-monoenergetic electron beam.

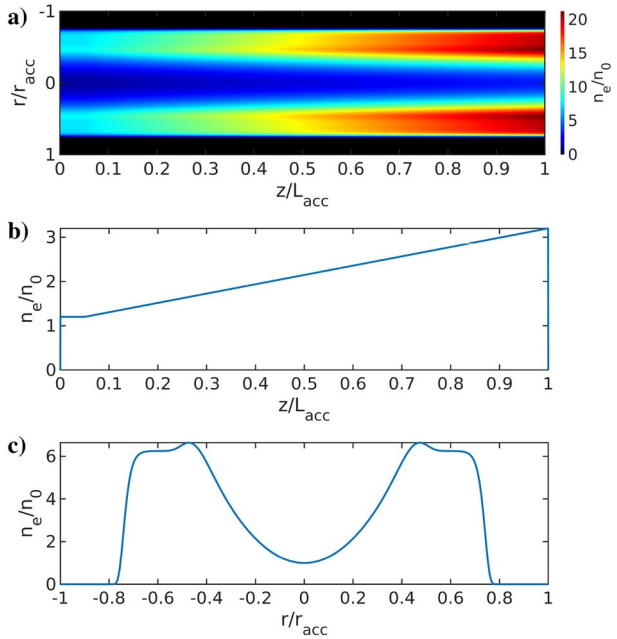

Fig. 2. Overview of the plasma density profiles used in simulations. All global injection simulations (continuous ionization injection gas along the entire plasma length) used the same normalized profiles. (**a**) Electron density as a function of r and z. (**b**) Electron density profile along z at r = 0. The electron density increases linearly by 3x from z = $0.05L_{acc}$ to L_{acc}. Note L_{acc} = 40 cm, 1.2 m, 3.2 m, and 9 m, for runs 1–4 respectively. The electron density starts above n_0 due to the presence of a 5% nitrogen dopant throughout the plasma. (**c**) Electron density along r at z = 0. Note the shape of this profile is the same for all values of z while the density increases linearly along z.

Run	E (J)	n_{e0} (cm^{-3})	r_0 (μm)	τ_0 (fs)	L_p (m)	Q(nC)	E_{max} (GeV)
1	13.8	8×10^{16}	30	75	0.27	1.1	13
2	39.0	4×10^{16}	42.4	106	0.78	2.2	26
3	110.4	2×10^{16}	60	150	2.1	3.4	52
4	312.3	1×10^{16}	84.9	212	6.1	4.9	104

Table 1. Table of simulation parameters and results for use as route to scale current 5–7 GeV LWFA experiments on CSU to 100 GeV.

Simulation results

The starting point of our Particle-In-Cell (PIC) simulations is the experiment on the ALEPH laser described in Miao et al.[9] with the main difference being the inclusion of a linear density up-ramp along the plasma waveguide to reduce the effects of dephasing. Figure 2 shows an overview of the plasma density profiles used in the simulations and a summary of the results demonstrating scaling to 100 GeV is shown in Table 1. In all the simulations we present the laser pulse evolution is similar, initially mode beating[39] in the channel occurs and the peak electric field increases as the pulse steepens. The laser pulse looses energy and undergoes red-shifting as it propagates[45]. Due to our use of a density up-ramp, the limiting factor in our simulations is pump depletion where the laser has catastrophic energy loss and red-shifting[46] around the distance L_p as given in Table 1.

We previously discussed how the scaling down of the density allows for increased electron acceleration. We have preformed this scaling 3 times for a total of 4 runs at successively lower densities. We continue decreasing the density from the original run by a factor of 2 until the desired peak electron energy as predicted in Eq. (1) of 100 GeV is reached. In this way a scaling of the energy gain, total charge in bunch, and length of plasma required to achieve this energy can be generated.

As described above, a key advantage of operating in the bubble regime is that filling the electron bucket with electrons can be done with the accelerating laser, provided that a small amount ($\sim 5\%$) of dopant gas (N_2 in our case) is introduced into the background gas that forms the plasma. Note that because the electron injection is complex and involves multiple non-linear processes, simulations are required to determine the resulting electron beam characteristics. In the simulations listed in Table 1, we initialize the background plasma as a fully ionized hydrogen gas with a 5% N^{+5} nitrogen gas dopant throughout the plasma. The N^{+6} and N^{+7} electrons are liberated near the peak laser electric field and hence are more easily injected into the accelerating phase of the

wake field. In our simulations the nitrogen dopant was critical as we saw no accelerated charge without it. This is because the hydrogen is easily ionized by the leading edge of the pulse, not the peak intensity, so freed electrons are not in the correct locations for ionization injection (something that is not true for gasses like nitrogen or argon). Our use of $\lambda_0 = 800$ nm and $a_0 = 2.2$ sets the laser field strength. Note that this electric field strength is an important factor in determining the threshold required for ionization injection using nitrogen gas. For example, $a_0 = 2.2$ and $\lambda_0 = 400$ nm yields no ionization injection.

We also ran simulationsf with a localized Nitrogen dopant layer that was 4 mm long, centered at $z = 1$ cm. While the localized injection method was able to achieve a higher maximum electron energy, the continuous injection method provided substantially more charge and the amount of charge was found to be consistent for both variants of simulations (quasi-3D RZ vs 3D cartesian) A comparison of the electron spectra from the localized injection and continuous injection methods is shown in figure 3.

In the simulations, the plasma waveguide was modeled as a parabolic guiding channel[15,47] given by the equation $n_e = n_{e0} a r^2$, with $a = 1/(\pi \cdot r_0^4 \cdot 2.81 \times 10^{-15})$. As discussed above, to reduce the effects of electron dephasing we employed a linear plasma density ramp along the laser axis. This axial linear density ramp both improves the electron energies and reduces the plasma length when compared to a constant axial density profile. We also performed simulations with a quadratic density profile but saw negligible improvements compared to the linear profile.

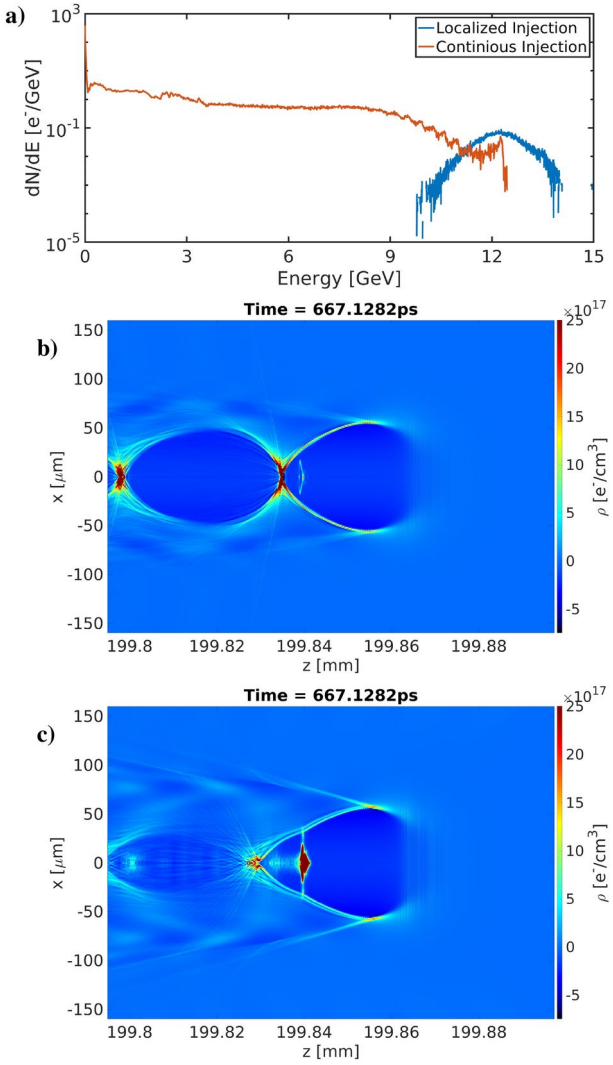

Fig. 3. (**a**) Comparison of simulations with a localized injection layer (blue) and continuous injection (red) for Case 1. The units of *dN*/*dE* are electrons/GeV. While the localized injection layer obtained the highest peak electron energy, the continuous injection method provides substantially more charge when considering total charge >9.9 GeV or lower energy. The localized injection method only provides 16 pC of total charge while the continuous injection method provides 1.1 nC of charge (above 1 GeV). Figures (**b**) and (**c**) Comparison of the charge density geometry of these simulations of localized injection (**b**) and continuous injection (**c**). Note that the continuous injection case undergoes beam loading, where the bubble structure of the wake is altered by the large accelerated electron charge.

Table 1 summarizes the simulations performed to develop a scaling of laser and plasma parameters from 10 GeV to 100 GeV. The columns are as follows: (1) The simulation run number, (2) the laser pulse energy as defined by $E[J] = 2.71 \times 10^{-5} \times (a_0 r_0/\lambda_0)^2 \tau_0[fs]$, (3) The on axis ionized hydrogen plasma density at the start of the simulation (note there was an additional 5% partially ionized nitrogen dopant), (4) the laser pulse spot size at best focus as defined by $E \propto e^{-(r/r_0)^2}$, (5) The laser pulse duration as defined by $E \propto e^{-(t/\tau_0)^2}$, (6) the distance at which the maximum electron energy was achieved, (7) the charge of electrons with energies above 1 GeV at the distance quoted in column 6, and (8) the maximum electron energy at the distance quoted in column 6.

Figure 4a shows the time history of the electron energy spectrum for "Run 4". Note the modulations in the high energy range are the result of a mode beating effect that occurs during ionization injection[39]. Figure 4c displays the accelerated electron charge for a given cutoff energy. In this case, the charge plotted is the total charge measured at the z-location $z = L_p$, when the maximum electron energy is obtained, with L_p listed in Table 1. It is noteworthy that the charge in the bunch for each simulation is a result of self-consistent beam loading.

Figure 5a displays the scaling for the peak electron energy, Fig. 5b the acceleration length, and Fig. 5c the total charge in the bunch as a function of laser energy that was obtained from the simulations. This slope of this scaling compares favorably with that given by the Lu scaling[26,27] which includes the guiding channel, the main difference being that the scaling found in this paper is improved in all three metrics. We observe a constant scaling enhancement in each of these quantities, for a given laser energy we find the electron energy scaled by a factor of 1.42, the required length by a factor of 0.6, and the accelerated charge by a factor of 4.2, when compared with the Lu scaling. This is readily explained by the fact that we have included a density up-ramp that increases the longitudinal electric field and helps the electrons to stay in phase slightly longer than the distance limit imposed by dephasing. In Fig. 5c the first data point from "Run 1" was excluded from the fit. We consider charge greater than 1GeV to be relevant to muon production, for the runs 2,3,4 this is a small fraction of the peak electron energy but for "Run 1" it is not. The scaling results presented here are empirically derived from somewhat idealized simulations where we have modeled the gas density profile with analytic functions. In experiments, imperfections in the density profile would likely negatively impact acceleration due to a mismatch in the laser-channel size, also imperfections could allow laser light to leak out of the channel.

Conversion to muons

The method of muon generation we are proposing originates with the GeV electron beam interacting with a high-Z converter target that has a physical dimension along the beam axis of $\gg$10 radiation lengths. This results in the electron losing $> e^{-10}$ of its original energy at these ultrarelativistic limits, and producing muons through Bethe–Heitler pair production or muons via pion decay. Detailed cross sections for muon generation as a function of incident electron energy can be found in[34]. Obtaining the highest possible electron energies is desirable as the peak muon energy is correlated to the peak electron energies and this maximum muon energy determines the amount of material that the muon can penetrate and therefore be useful for imaging. Similarly, When considering the entire spectrum of the muons generated, the flux at various energies will determine the strength of the muon source for the corresponding amounts of material that can be penetrated. Referring back to Fig. 3, a finite layer of dopant gas used as an injection layer will yield a higher energy muon and thus allow for imaging through more (or denser) material, whereas having gas dopant fill the entire accelerator yields higher

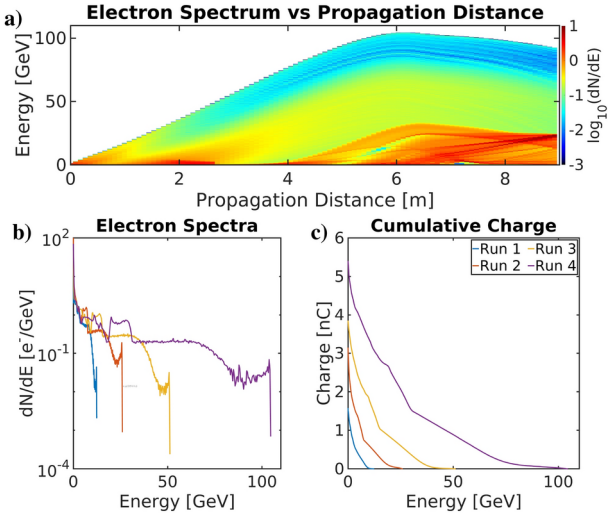

Fig. 4. (**a**) Electron energy spectrum vs laser propagation distance for the 104 GeV simulation "Run 4". (**b**) Electron energy spectrum at peak energy for each simulation. The units of *dN*/*dE* are electrons/GeV. The line corresponding to "Run 4" is essentially a line-out of panel (**a**) at 6.12 m. (**c**) Total accelerated electron charge above the specified energy at peak energy for each simulation.

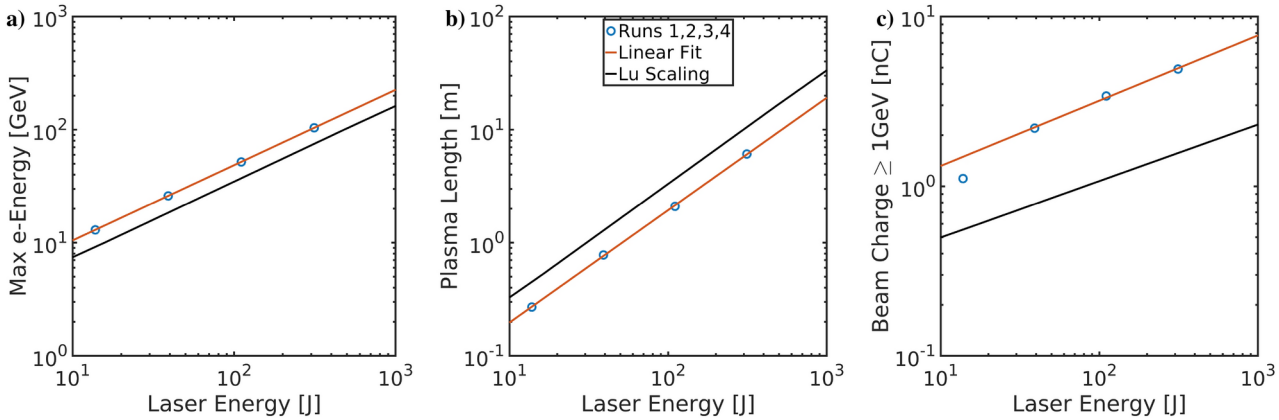

Fig. 5. **Left:** Scaling of peak electron energy as a function of laser energy for LWFA in the blowout regime. **Center:** Scaling of the plasma length required as a function of laser energy. **Right:** Scaling of amount of charge in the beam for all electrons with energy over 1 GeV as a function of laser energy for LWFA in the blowout regime. Note for this plot the first data point from "Run 1" was excluded from the fit, see text for details. For all plots the black solid scaling is from Lu et al.[26,27] for a0 = 1.76 in the case of a preformed channel. Scaling found from simulation (including a linear density up ramp) is shown in red.

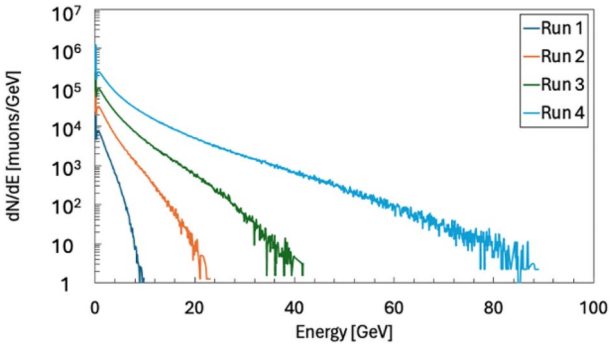

Fig. 6. Muon spectra resulting from FLUKA simulations with input electron spectra from WarpX simulations.

flux for all energies below the peak energy, but the peak is roughly 10% lower than the finite thickness injection layer case.

The FLUKA Monte Carlo transport code[48–50] (version 4-3.3) is used to estimate the muon source strength for the simulated electron spectra shown above in Fig. 4b. The electron spectra from Fig. 4b are sent into a 2 cm thick Tungsten converter which is unoptimized and exceeds the expected ideal thickness of 2 radiation lengths predicted from theory[51]. The resulting combined muon+ and muon- particle spectra for all 4 LWFA simulations are shown in Fig. 6. Note that the maximum muon energy is approximately 10% lower than that of the corresponding electron maximum energy. From these results, we can estimate the total number of muons that can be generated generated for a single laser pulse. For example, using Fig. 4b to estimate the number of primary electrons for the 104GeV case, we find that 8.97×10^5 total muons would have been generated for the spectra shown in Fig. 6 corresponding to Run 4. These muons are predominantly directed in the forward direction.

Conclusions

A series of 3D PIC simulation results were presented and used to demonstrated the feasibility of scaling an existing experiment[9] to electron energies up to 100 GeV containing greater than 1 nC of charge per bunch. For the case where the peak electron energy reaches 100 GeV, this would require a single laser pulse of approximately 310 J with a spot size of 85 microns, and a plasma length of approximately 6 m. Bessel beam propagation and hydrocode simulations have already demonstrated the feasibility of meter-scale waveguides, where a 1J laser was shown to generate a 1-m plasma waveguide suitable for LWFA[52,53].

Based on FLUKA simulations that used the simulated electron bunches as an input, approximately 10^4-10^6 muons/pulse can be generated for use in imaging. If these yields were to be generated from a laser with a repetition rate of 1/minute, they would match or exceed the average flux of cosmic muons (1/cm^2/min). Next generation ultrafast laser drivers are projected to be capable of producing suitable driver pulses at tens to hundreds of kilowatts average power[54–57]. For example, the Tm:YLF-based architecture was recently demonstrated to

produce high energy fs-duration pulses[58] and pulse energies in excess of 100 J[59] in a compact, all-diode-pumped amplifier. This driver technology is projected to scale to 300 J at kHz repetition rates and therefore , and therefore a frequency-doubled implementation of this system could provide $\sim 10^4$ times more muons per bunch than the cosmic ray source. For reference, the highest energy muons in the tail of the distribution, those greater than 50 GeV as seen in Run 4, can penetrate up to 100 m of compacted soil. Assuming theses bunches are created by an accelerator driven by a laser with the average power projected to be achievablein the near future that fits in a small footprint, the entire accelerator and muon target could enable a transportable, active muon source with fluences significantly larger than that generated by cosmic rays.

Methods

Simulations were performed using the Particle-In-Cell (PIC) code WarpX[60]. In order to propagate the laser for several meters, the Lorentz boosted frame algorithm[61] and spectral solver[62,63] was required. The simulations had a typical resolution of $1\mu m$ in the transverse and $0.5\mu m$ in the longitudinal direction, however in the boosted frame the laser is stretched by a factor of γ_{boost} along its propagation direction so that its wavelength is well resolved with our values of $\gamma_{boost} = 10 - 40$.

We performed 3D Cartesian and quasi-3D[64] (cylindrical with azimuthal mode decomposition) simulations which demonstrated consistent results. We typically used 4 Particles-Per-Cell (PPC) in the 3D Cartesian simulations and 64 PPC in the quasi-3D simulations. Our 3D Cartesian simulations (c.f. Fig. 1) were used to validate the quasi-3D simulations which were used for the main scaling results reported here. The quasi-3D simulations model the fields in RZ with the addition of 3 azimuthal modes included[65]. The first mode is required to capture the plasma waves and the second mode is required to include the laser polarization[64]. We find that additional modes better capture pulse evolution dynamics and beam instabilities which are not necessarily symmetric. Simulation Case 1 was run in both 3D Cartesian and quasi-3D. We found that the history of the accelerated electron energies, acceleration lengths, and charge in the electron bunch were nearly identical for the two cases.

Data availability

The datasets used and/or analysed during the current study are available from the corresponding author on reasonable request.

Received: 22 November 2024; Accepted: 20 March 2025
Published online: 17 July 2025

References

1. Alvarez, L. W. et al. Search for hidden chambers in the pyramids. *Science* **167**(3919), 832–839 (1970).
2. Morishima, K. et al. Discovery of a big void in Khufu's pyramid by observation of cosmic-ray muons. *Nature* **552**, 386–390 (2017).
3. Fujii, H. et al. Performance of a remotely located muon radiography system to identify the inner structure of a nuclear plant. *Prog. Theor. Exp. Phys.* **2013**(7), 073C01 (2013).
4. Patnaik, R., Lee, Y. & Dorroh, D. Image based object identification in muon tomography. In *2014 IEEE Nuclear Science Symposium and Medical Imaging Conference (NSS/MIC)* 1–9 (2014).
5. Accettura, C. et al. Towards a muon collider. *Eur. Phys. J.* **83**, 864 (2023).
6. Tajima, T. & Dawson, J. M. Laser electron accelerator. *Phys. Rev. Lett.* **43**, 267–270 (1979).
7. Aniculaesei, C. et al. The acceleration of a high-charge electron bunch to 10 GeV in a 10-cm nanoparticle-assisted wakefield accelerator. *Matter Radiat. Extremes* **9**(1), 014001 (2023).
8. Gonsalves, A. J. et al. Petawatt laser guiding and electron beam acceleration to 8 GeV in a laser-heated capillary discharge waveguide. *Phys. Rev. Lett.* **122**, 084801 (2019).
9. Miao, B. et al. Multi-GeV electron bunches from an all-optical laser wakefield accelerator. *Phys. Rev. X* **12**, 031038 (2022).
10. Bobbili Sanyasi, R., Jong Ho, J., Hyung Taek, K. & Chang Hee, N. Bright muon source driven by GeV electron beams from a compact laser wakefield accelerator. *Plasma Phys. Controll. Fusion* **60**(9), 095002 (2018).
11. Dreesen, W. et al. Detection of petawatt laser-induced muon source for rapid high-z material detection. In *2014 IEEE Nuclear Science Symposium and Medical Imaging Conference (NSS/MIC)* 1–6 (2014).
12. Calvin, L. et al. Laser-driven muon production for material inspection and imaging. *Front. Phys.* **11**, 1177486 (2023).
13. Martins, S. F., Lu, W., Fonseca, R. A., Mori, W. B. & Silva, L. O. Exploring laser-wakefield-accelerator regimes for near-term lasers using particle-in-cell simulation in Lorentz-boosted frames. *Nat. Phys.* **6**(4), 311–316 (2010).
14. Kiani, L. et al. High average power ultrafast laser technologies for driving future advanced accelerators. *J. Instrum.* **18**(08), T08006 (2023).
15. Durfee, C. G. & Milchberg, H. M. Light pipe for high intensity laser pulses. *Phys. Rev. Lett.* **71**, 2409–2412 (1993).
16. Miao, B., Feder, L., Shrock, J. E., Goffin, A. & Milchberg, H. M. Optical guiding in meter-scale plasma waveguides. *Phys. Rev. Lett.* **125**, 074801 (2020).
17. Feder, L., Miao, B., Shrock, J. E., Goffin, A. & Milchberg, H. M. Self-waveguiding of relativistic laser pulses in neutral gas channels. *Phys. Rev. Res.* **2**, 043173 (2020).
18. Shrock, J. E., Miao, B., Feder, L. & Milchberg, H. M. Meter-scale plasma waveguides for multi-GeV laser wakefield acceleration. *Phys. Plasmas* **29**(7), 073101 (2022).
19. Picksley, A. et al. Matched guiding and controlled injection in dark-current-free, 10-GeV-class, channel-guided laser-plasma accelerators. *Phys. Rev. Lett.* **133**, 255001 (2024).
20. Sprangle, P. et al. Wakefield generation and GeV acceleration in tapered plasma channels. *Phys. Rev. E* **63**, 056405 (2001).
21. Guillaume, E. et al. Electron rephasing in a laser-wakefield accelerator. *Phys. Rev. Lett.* **115**, 155002 (2015).
22. Geddes, C. G. R. et al. High-quality electron beams from a laser wakefield accelerator using plasma-channel guiding. *Nature* **431**, 538–541 (2004).
23. Faure, J. et al. A laser-plasma accelerator producing monoenergetic electron beams. *Nature* **431**, 541–544 (2004).
24. Mangles, S. P. D. et al. Monoenergetic beams of relativistic electrons from intense laser-plasma interactions. *Nature* **431**, 535–538 (2004).
25. Albert, F. et al. Laser wakefield accelerator based light sources: Potential applications and requirements. *Plasma Phys. Control. Fusion* **56**, 084015 (2014).

26. Lu, W. et al. Generating multi-GeV electron bunches using single stage laser wakefield acceleration in a 3D nonlinear regime. *Phys. Rev. ST Accel. Beams* **10**, 061301 (2007).
27. Lu, W., et al. Designing LWFA in the blowout regime. In *2007 IEEE Particle Accelerator Conference (PAC)* 3050–3051 (2007).
28. Ekerfelt, H., Hansson, M., Gallardo González, I., Davoine, X. & Lundh, O. A tunable electron beam source using trapping of electrons in a density down-ramp in laser wakefield acceleration. *Sci. Rep.* **7**, 12229 (2017).
29. Bulanov, S., Naumova, N., Pegoraro, F. & Sakai, J. Particle injection into the wave acceleration phase due to nonlinear wake wave breaking. *Phys. Rev. E* **58**, R5257–R5260 (1998).
30. Pak, A. et al. Injection and trapping of tunnel-ionized electrons into laser-produced wakes. *Phys. Rev. Lett.* **104**, 025003 (2010).
31. Chen, M., Sheng, Z.-M., Ma, Y.-Y. & Zhang, J. Electron injection and trapping in a laser wakefield by field ionization to high-charge states of gases. *J. Appl. Phys.* **99**(5), 056109 (2006).
32. Stanev, T. & Vankov, C. P. Production of high-energy muons in gamma showers. *Phys. Lett. B* **158**(1), 75–76 (1985).
33. Stanev, T., Vankov, C. P. & Halzen, F. Muons in gamma showers. In *19th International Cosmic Ray Conference (ICRC19), International Cosmic Ray Conference*, Vol. 7, 219 (1985).
34. Motz, J. W., Olsen, H. A. & Koch, H. W. Pair production by photons. *Rev. Mod. Phys.* **41**, 581–639 (1969).
35. Bulanov, S. V. et al. On the problems of relativistic laboratory astrophysics and fundamental physics with super powerful lasers. *Plasma Phys. Rep.* **41**(1), 1–51 (2015).
36. Bulanov, S. V. et al. On some theoretical problems of laser wake-field accelerators. *J. Plasma Phys.* **82**(3), 905820308 (2016).
37. Wang, Y. et al. 0.85 micron pw laser operation at 3.3 khz and high-contrast ultrahigh-intensity nm second-harmonic beamline. *Opt. Lett.* **42**(19), 3828–3831 (2017).
38. Miao, B., Shrock, J. & Milchberg, H. Electrons see the guiding light. *Phys. Today* **76**(8), 54–55 (2023).
39. Shrock, J. E. et al. Guided mode evolution and ionization injection in meter-scale multi-GeV laser wakefield accelerators. *Phys. Rev. Lett.* **133**, 045002 (2024).
40. Titov, A. I., Kämpfer, B. & Takabe, H. Dimuon production by laser-wakefield accelerated electrons. *Phys. Rev. ST Accel. Beams* **12**, 111301 (2009).
41. Aniculaesei, C. et al. Electron energy increase in a laser wakefield accelerator using up-ramp plasma density profiles. *Sci. Rep.* **9**(1), 11249 (2019).
42. Katsouleas, T. Physical mechanisms in the plasma wake-field accelerator. *Phys. Rev. A* **33**, 2056–2064 (1986).
43. Private communication, Ela Rockafellow.
44. Ralph, J. E. et al. Self-guiding of ultrashort, relativistically intense laser pulses through underdense plasmas in the blowout regime. *Phys. Rev. Lett.* **102**, 175003 (2009).
45. Hussein, A. E. et al. Direct spectral measurements of midinfrared radiation from a laser wakefield accelerator. *Phys. Rev. A* **106**, 063505 (2022).
46. Shadwick, B. A., Schroeder, C. B. & Esarey, E. Nonlinear laser energy depletion in laser-plasma acceleratorsa). *Phys. Plasmas* **16**(5), 056704 (2009).
47. Clark, T. R. & Milchberg, H. M. Optical mode structure of the plasma waveguide. *Phys. Rev. E* **61**, 1954–1965 (2000).
48. Ahdida, C. et al. New capabilities of the fluka multi-purpose code. *Front. Phys.* **9**, 788253 (2022).
49. Battistoni, G. et al. Overview of the fluka code. *Annals Nucl. Energy* **82**, 10–18 (2015). Joint International Conference on Supercomputing in Nuclear Applications and Monte Carlo 2013, SNA + MC 2013. Pluri- and Trans-disciplinarity, Towards New Modeling and Numerical Simulation Paradigms.
50. Fluka website: https://fluka.cern
51. Tsai, Y.-S. Pair production and bremsstrahlung of charged leptons. *Rev. Mod. Phys.* **46**, 815–851 (1974).
52. Miao, B. et al. Measurements and simulations of hydrodynamic plasma waveguides generated by optical field ionization. arXiv:2404.13632 (2024).
53. Gordon, D.F., Sprangle, P., Slinker, S., Fernsler, R. & Lampe, M. Sparc- A simulation model for electrical discharges. *NRL Memorandum Report*, 6790-06 (2006).
54. Wang, Y. et al. 1.1 J Yb:YAG picosecond laser at 1 khz repetition rate. *Opt. Lett.* **45**(24), 6615–6618 (2020).
55. Rainville, A., Chen, M., Whittlesey, M., Du, Q. & Galvanauskas, A. 22mj coherent beam combining from three 85μm core ccc fiber amplifiers. In *Conference on Lasers and Electro-Optics, SW2B.4* (Optica Publishing Group, 2021).
56. Chen, S. et al. Broadband spectral combining of three pulse-shaped fiber amplifiers with 42fs compressed pulse duration. *Opt. Express* **31**(8), 12717–12724 (2023).
57. Sistrunk, E. et al. Laser technology development for high peak power lasers achieving kilowatt average power and beyond. In *Short-Pulse High-energy Lasers and Ultrafast Optical Technologies*, Vol. 11034 (eds Bakule, P. & Haefner, C. L.) 1103407 (International Society for Optics and Photonics, SPIE, 2019).
58. Tamer, I. et al. Demonstration of a 1 TW peak power, joule-level ultrashort Tm:YLF laser. *Opt. Lett.* **49**(6), 1583–1586 (2024).
59. Tamer, I. et al. 1 GW peak power and 100 j pulsed operation of a diode-pumped Tm:YLF laser. *Opt. Express* **30**(26), 46336–46343 (2022).
60. Fedeli, L., Huebl, A., Boillod-Cerneux, F., Clark, T., Gott, K., Hillairet, C., Jaure, S., Leblanc, A., Lehe, R., Myers, A. and Piechurski, C., Sato, M., Zaim, N., Zhang, W., Vay, J.-L. & Vincenti, H. Pushing the frontier in the design of laser-based electron accelerators with groundbreaking mesh-refined particle-in-cell simulations on exascale-class supercomputers. In *SC22: International Conference for High Performance Computing, Networking, Storage and Analysis* 1–12 (2022).
61. Vay, J.-L. Noninvariance of space- and time-scale ranges under a Lorentz transformation and the implications for the study of relativistic interactions. *Phys. Rev. Lett.* **98**, 130405 (2007).
62. Lehe, R., Kirchen, M., Godfrey, B. B., Maier, A. R. & Vay, J.-L. Elimination of numerical Cherenkov instability in flowing-plasma particle-in-cell simulations by using Galilean coordinates. *Phys. Rev. E* **94**, 053305 (2016).
63. Kirchen, M. et al. Stable discrete representation of relativistically drifting plasmas. *Phys. Plasmas* **23**(10), 100704 (2016).
64. Lifschitz, A. F. et al. Particle-in-cell modelling of laser-plasma interaction using Fourier decomposition. *J. Comput. Phys.* **228**(5), 1803–1814 (2009).
65. Lehe, R., Kirchen, M., Andriyash, I. A., Godfrey, B. B. & Vay, J.-L. A spectral, quasi-cylindrical and dispersion-free particle-in-cell algorithm. *Comput. Phys. Commun.* **203**, 66–82 (2016).

Acknowledgements

This work was supported by the Defense Advanced Research Program Agency (DARPA) under the Muons for Science and Security Program. This work was performed under the auspices of the U.S. Department of Energy by Lawrence Livermore National Laboratory under Contract DE-AC52-07NA27344. Computing support for this work came from the Lawrence Livermore National Laboratory (LLNL) Institutional Computing Grand Challenge program. The Maryland authors acknowledge the U.S. Department of Energy (DE-SC0015516, Laser-NetUS DE-SC0019076/FWP SCW1668, and DE-SC0011375), the National Science Foundation (PHY2010511), and NSF GRFP (Grant No. DGE 1840340). The Lawrence Berkeley National Laboratory authors work was performed under Contract No. DE-AC02-05CH11231 with the U.S. Department of Energy. The authors would like to thank J. Liptac, M. Wrobel, T. Dodson, C. Benedetti, A. Longman, G. Grittani, I. Tamer, J. Rocca, V. Shlyaptsev,

and J. Harton for useful discussions.

Author contributions

The project was conceived by J.L., S.W., A.K., V.T., and B.R. Theoretical work was performed by J.L., S.W., A.K. and B.R. The WarpX simulations were performed by J.L. with support from A.K., J.V., A.H, R.L. and E.R. The FLUKA simulations were performed by A.C. and R.V. The paper was written by J.L. and S.W. with assistance from G.W., A.K, R.V., N.L., E.R., B.M., J.S., H.M., J.V., A.H, R.L., A.C., R.V., S.B, P.V, V.T., and B.R. All the authors read and approved the paper.

Declarations

Competing interests

The authors declare no competing interests.

Additional information

Correspondence and requests for materials should be addressed to J.D.L.

Reprints and permissions information is available at www.nature.com/reprints.

Publisher's note Springer Nature remains neutral with regard to jurisdictional claims in published maps and institutional affiliations.

Open Access This article is licensed under a Creative Commons Attribution-NonCommercial-NoDerivatives 4.0 International License, which permits any non-commercial use, sharing, distribution and reproduction in any medium or format, as long as you give appropriate credit to the original author(s) and the source, provide a link to the Creative Commons licence, and indicate if you modified the licensed material. You do not have permission under this licence to share adapted material derived from this article or parts of it. The images or other third party material in this article are included in the article's Creative Commons licence, unless indicated otherwise in a credit line to the material. If material is not included in the article's Creative Commons licence and your intended use is not permitted by statutory regulation or exceeds the permitted use, you will need to obtain permission directly from the copyright holder. To view a copy of this licence, visit http://creativecommons.org/licenses/by-nc-nd/4.0/.

© The Author(s) 2025